Production Engineering (2026) 20:50
https://doi.org/10.1007/s11740-026-01427-5

ORIGINAL PAPER

Reinterpretation and demonstration of deformation ageing in cold-formable steels

Béla Kondás[1] · Zoltán Péter Kovács[2] · Tamás Bubonyi[1] · Máté File[3] · Dániel Nemes[3] · Valéria Mertinger[1]

Received: 10 August 2025 / Accepted: 13 January 2026

Abstract
Many processing companies use some grades of steel for cold forming. Due to ageing, the formability of unalloyed mild steel sheets deteriorates over time; their formability is not uniform, and surface defects appear, which in many practical applications leads to scrap. This can be particularly important for processing companies when selecting machine settings, as there may be differences in the properties of materials from different manufacturers and the properties of materials of different ages from the same manufacturer. We investigated the ageing behaviour of DC01 steel grade by testing many samples from the third day after production up to one year. Various methods were used to detect ageing, such as tensile tests at different test speeds and supplemented with a digital image correlation (DIC) system, thermo-electric power measurement, deep drawing cup tests, and Nakajima tests. We showed that a reinterpretation of the definition of ageing is necessary. Standard tensile testing can no longer detect the ageing tendency of steels manufactured using the latest technology. However, when supplemented with DIC, these tests show ageing with high sensitivity. Among the used methods the applicability of this technique in industrial material testinglaboratories is the most recommended.

Keywords Mild steel · Strain ageing · Digital image correlation · Tensile testing · Formability · Forming limit curve

1 Introduction

Variation of mechanical properties of steel sheets greatly influences processing parameters and the final product quality. The scattering effect was caused, among others by less robust sheet manufacturing technology and ageing phenomena of the steel sheets [1]. The ageing of steels is extremely detrimental to the formability of sheet metal because their dynamic and impact is almost unpredictable. This phenomenon has been known for a long time. The basic metallurgical relationships were established in the 1940s [2] and 1950s [3]. Deep drawable steel sheets was a popular product during the post-World War II reindustrialisation, so much scientific research on ageing was conducted in the 1960s [4], 1970s and 1980s [5]. With the advancement of technology, improved versions of low-carbon (LC) [6] steels, known as microalloyed (bake hardening BH [7], Dual Phase DP [8], Complex Phase CP [9], Transformation Induced Plasticity (TRIP) [9] etc.) steels, appeared on the market in the 1990s, primarily to meet the automotive industry's requirements. All of these new types of steels suffer from the ageing effect. The ageing phenomenon is caused by the pinning effect of dislocations in the iron lattice's interstitial atoms (C, N). At

✉ Valéria Mertinger
valeria.mertinger@uni-miskolc.hu

Béla Kondás
bela.kondas@uni-miskolc.hu

Zoltán Péter Kovács
peter.kovacs@uni-miskolc.hu

Tamás Bubonyi
tamas.bubonyi@uni-miskolc.hu

Máté File
mate.file@eng.unideb.hu

Dániel Nemes
nemes.daniel@eng.unideb.hu

[1] Faculty of Materials and Chemical Engineering, Institute of Physical Metallurgy, Metalforming and Nanotechnology, University of Miskolc, Miskolc, Hungary

[2] Faculty of Mechanical Engineering and Information Technology, Institute of Materials Science and Technology, University of Miskolc, Miskolc, Hungary

[3] Faculty of Engineering, Department of Mechanical Engineering, University of Debrecen, Debrecen, Hungary

Published online: 18 February 2026

the beginning of forming the sheets, the dislocations break away from these atoms, which requires greater force. Once the breakage has occurred, even lower forces are sufficient to cause further movement of the dislocations. This phenomenon causes the appearance of lower and upper yield points on the tensile diagram (static strain ageing) [10]. A dynamic version of ageing develops after the start of plastic deformation when the diffusion velocity of the interstitial atoms becomes high enough to follow the movement of the dislocations, especially when the deformation speed is not too high. At this point, the moving cloud is sufficiently extensive to significantly impede the further movement of the dislocations (dynamic strain ageing). Diffusion depends primarily on the time available, so the number of atoms reaching the dislocations increases as a function of the relaxation time after deformation. As a result of ageing, the proof strength and tensile strength increase, but the elongation decreases. Hrivnák and Sobotová [6] measured an increase in yield strength of approximately of 38 MPa, and Bhagat [11] measured an increase of 26–37 MPa after the performed ageing. Artificial ageing using heat treatment can also accelerate ageing processes [12]. Subsequently, the increase in the proof strength after treatment is examined, which is measured by the Strain Ageing Index (SAI). Bhagat, Baek and Lee [11] conducted extensive studies to determine the SAI of materials. In their article, the specimens were pulled up to 7.5% strain, and the proof strength (Rp0.2e) was recorded. The specimens were treated at 100 °C for 60 min, pulled till fracture, and the proof strength was re-recorded (Rp0.2u). The SAI Index was determined as follows (1).

$$\mathrm{SAI} = \mathrm{Rp0.2u} - \mathrm{Rp0.2e} \tag{1}$$

From a practical point of view, changes in mechanical properties may increase the risk of cracking during sheet forming and cause other surface issues. These include Potrevin-Le Chatelier (PLC) effect [13] and Lüders lines [14].

The tensile test extended by the Digital Image Correlation (DIC) technique can successfully detect these effects. However, its only disadvantage is the large amount of data and the time required for its evaluation. Although the procedure is not yet standardised, the DIC technique is widely used for research on metal sheets [15]. The essence of the process is that a calibrated camera system records the image of a random pattern (speckles) applied to the surface of the test specimens during the test, and the matched software evaluates the distortion of the unique pattern. Using the pattern, the system evaluates the local strainsoccurring on the test specimen and displays it on a scaled colour diagram (strain map). The strain map provides a precise indication of the unevenness of the deformation in the area of the test specimen detected by the camera. Halim et al. investigated the PLC effect [16], and Qiu et al. analysed the formation of Lüders lines [17]. Both are typical signs of dynamic strain ageing.

Another way to study ageing is to examine not only the effect, i.e. the change in mechanical properties, but also the location of the alloying elements. One method for this is to measure the change in thermoelectric power [18]. The test principle is based on the observation that if the two ends of a test sample are set to two different temperatures, a potential difference arises between the two ends due to the temperature difference [19]. The thermoelectric power (TEP) or so-called Seebeck coefficient (S) is defined as the ratio of the thermoelectric voltage (U) to the temperature difference (ΔT) [20] (2).

$$\mathrm{S} = \frac{\mathrm{U}}{\Delta \mathrm{T}} \tag{2}$$

If, due to diffusion, the interstitial elements (e.g. N and C) migrate to a state of equilibrium, the test sample's thermoelectric power increases. Mucsi suggested using this technique for ageing [21]. He used thermoelectric power measurements on steel plates to demonstrate the precipitation of nitrides during production. According to his data, after heat treatment at 120 °C for 60 min (corresponding to approximately 40 weeks of storage), the TEP increase was 160 nV/K.

Standardised test procedures are widely used in industrial practice to provide numerical values for the formability of sheets without investigating the causes. Typical tests include the deep drawing cup test (ISO 11531) and the Nakajima test (EN ISO 12004-2).

European standards distinguish between several types of steels for cold forming, of which DC01 is the entry-level grade. This grade does not contain any nitrogen-binding alloying elements other than aluminium. The carbon and nitrogen atoms, which play the most important role in ageing, are located interstitially in the ferrite lattice. They have a high diffusion coefficient and are therefore capable of movement, so ageing can be expected even when stored in an industrial environment. The mechanical properties of DC01 steel are specified in EN 10,130 standard. A study of this standard reveals some peculiarities that may be related to ageing. For example, the proof strength is only guaranteed for 8 days, while the specified tensile strength and elongation values are not guaranteed. The standard also states that the tendency for stretcher strains to appear on the surface of sheets increases "after a certain period of time," so it is recommended that DC01 products be processed within 6 weeks of delivery. Comparing the above data with the stability of the product properties of other standard steel

grades, it can be stated that ageing is expected to occur most rapidly in DC01 quality, making it ideal for studying ageing behaviour.

Previous research has studied the nature of ageing based on standard tensile tests at normal and reduced test speeds. Normal test speed is as prescribed in the ISO 6892-1 standard; however, the reduced test speed is significantly lower than the standard suggested. Finally, the ageing was associated with the increase of proof and tensile strength, the decrease in elongation, the appearance of lower and upper yield points (static ageing), and the appearance of serration in the tensile diagram (dynamic ageing). In our experience, these parameters did not indicate ageing processes in numerous complaints regarding the shaping of mild steel. Our research aimed to conduct a comprehensive analysis that provides a detailed picture of the nature and dynamics of the ageing of mild steels, and to develop a method that can be applied in industrial practice as a reliable method for detecting strain ageing in these steels, thereby improving customer satisfaction.

2 Experimental

2.1 Material

The effects of ageing were studied on samples of DC01 grade, 1.5 mm thick, cold-rolled, batch annealed, and skin passed coils from a European manufacturer. The different tests were carried out after production (skin pass rolling). The time intervals were determined based on relevant historical and today's national and international product standards. The test specimens were cut from at least 10 m from the end of the coil along the halfway between the centre and the outer edge of the coil as rolled, cutting them close to each other to minimise any inhomogeneity resulting from the coil manufacturing process.

Since preliminary information from the literature indicated that strain ageing is a complex phenomenon, we wanted to confirm the conclusions drawn from our experiments (1st round) with a 2nd series of tests (2nd round), using samples from two different batches (Table 1). While in the 1st round of tests, the samples aged naturally under industrial storage conditions (15–25 °C), in the 2nd round, except for the 3-day samples, the other samples were artificially aged by heat treatment recommended in [22]. According to this, 1 week of ageing was achieved by maintaining the temperature at 120 °C for 2.5 min. Accordingly, the tests were performed after 3 days (3dy), 9 days (9dy), 2,4,6,10 weeks (2,4,6,10 ws), 3, 6, 8,12 months (3,6,8,12 ms) of ageing.

2.2 Characterisation procedures

In order to map the nature of the ageing phenomenon as accurately as possible, we conducted additional tests simultaneously with the normal and reduced speed tensile tests. The 1st round tests aimed to reproduce the ageing phenomena described in the literature based on normal and reduced speed tensile tests, while the 2nd round tests aimed to find the most reliable method for predicting ageing.

2.2.1 Normal and reduced speed tensile tests

Ageing manifests in mechanical material testing characteristics, so tensile testing is the most widely used method. Here, it is critical to measure changes in mechanical properties with sufficient accuracy, i.e., to eliminate other influencing factors like test specimen preparation methods. For this reason, we use different methods and, within this, different test speeds to measure the change in mechanical properties (combined effect of static and dynamic ageing) and the graphical changes in the stress-strain diagram (effect of dynamic ageing). All significant influencing factors were kept at the same level during the experiments. We performed the tests with a calibrated tensile test machine. The calibration was performed for force, displacement, speed, longitudinal, and transversal strain according to ISO 9513 and 75,001. The measurement error of the measuring system was checked by testing reference specimens with certified mechanical values before each series of measurements. The normal and reduced speed tensile tests were only started when the measurement results of the reference sample matched the mechanical values specified in its certificate of conformity.

We examined three test specimens taken from three directions (with rolling directions of 0°, 45° and 90°) per measurement. The normal and reduced tensile tests were performed on specimens of standard size (ISO 6892-1 (18), 2 type (20 × 80 mm)), which were prepared by punching and grinding. The tensile tests were performed on an Instron 68FM-300 floor-mounted, dual-column universal testing machine using a manual wedge grip with electromechanical control. The eccentricity error between the applied load and the longitudinal axis of symmetry of the test specimen was reduced to a moderate extent using an alignment

Table 1 Chemical composition of steel [w%]

	C	Mn	*P*	S	Al	*N*
1st round	0.07	0.39	0.015	0.001	0.038	0.004
2nd round	0.07	0.43	0.013	0.001	0.046	0.003

piece mounted on the grips. The measurement results were obtained using Bluehill 4/AverEdge 32 evaluation software. During the test, the elongation of the specimens was measured using an AVE 2 video extensometer with an original gauge length of 80 mm in the longitudinal direction and 20 mm in the transverse direction. Further test parameters: Load cell: 300 kN; Test temperature: room temperature (23 ± 5 °C). The changes in mechanical properties (Rp0.2, ReH, ReL, Rm, A80) were examined for each series by normal test speed using the ISO 6892 B (stress control) method. The test speed (here: stress rate) was uniformly 10 MPa/s until the yield point appeared, and then 0.00671 s^{-1}. The appearance of the yield point and any graphical changes in the stress-strain diagram were tested by reduced speed test using the ISO 6892 A1 strain control method with three test speeds (here: strain rates) in each direction (0.002 s^{-1}; 0.0002 s^{-1}; 0.00002 s^{-1}). The same data sampling frequency (50 MHz) was used for all normal and reduced speed tensile tests.

We also used this equipment to determine the SAI index. We performed the tests using the ISO 6892 B (stress control) method at a stress rate of 10 MPa/s and evaluated the results following the EN 10,325 guidelines. The test specimen was taken transverselyto the rolling direction.

2.2.2 Tensile testextended by DIC technique

The size and preparation method of the test specimens prepared for DIC tensile testing were the same as those for standard tensile test specimens. One test specimen was taken at each time interval transversal to the rolling direction (90°). The specimen's surface was cleaned with Loctite SF 7063 solution, then primed with white AESUB paint, and finally, the speckle pattern was applied with Acryl Prisma Colour digitising spray. The extent of local strain changes was determined for each test specimen using the local inhomogeneity factor Λ [%], by the (3) formula [23].

$$\Lambda = \frac{\epsilon_{\max} - \epsilon_{\min}}{\epsilon_{av}} 100 \quad (3)$$

Where: ε_{max},ε_{min},ε_{av} maximum, minimum and average strain measured at a given moment of displacement.

The strain distribution pattern and the local inhomogeneity factor quantifying it were determined at the strain value corresponding to the yield point and at the value corresponding to 10% strain in the uniform plastic strain range at each ageing time interval. Static ageing was evaluated in the image corresponding to the yield point, while dynamic ageing was evaluated in the image corresponding to 10% strain. The tensile tests were performed on an Instron 68TM-10 table-mounted universal testing machine using a manual wedge grip with electromechanical control. The local strains were measured using a GOM Aramis 12 M-500 camera. The camera had a resolution of 12 megapixels. The data sampling frequency was 4 Hz. The measurement results were processed using Aramis Professional 2020 evaluation software. The Aramis parameters were as follows: facet size: 15 pixel; pointdistance: 12 pixel; computation: high accuracy; strain tensor neighborhood: 1; interpolation size: 0. Additional test parameters: Load cell: 10 kN; Test temperature: room temperature (23 ± 5 °C). The tests were performed with crosshead speed control. The test speed (here: crosshead separation rate) was 5 mm/min. The image analysis system was calibrated with a CP40/170 reference image before each measurement.

2.2.3 Micro tensile test

The tests were performed using a DEBEN material testing device integrated into a YXLON FF35 Computer Tomograph (CT). The design of the test specimen is shown in Fig. 1. The essence of the micro tensile test integrated into the CT device is that the failure can be observed on a test specimen, and the measurement area is much smaller (10 × 5 mm) than the standard 20 × 80 mm tensile test specimen. Our aim in using this test method was to investigate whether the small test specimen reacts more sensitively to the passage of time and whether any static or dynamic ageing signs that may occur are easier to read from the displacement diagram. As there is no approved standard for the test procedure, the test specimens were prepared by milling and drilling following the recommendations of the test machine manufacturer. The original gauge length was 5 mm. The test specimens were machined transversely to the rolling direction (90°). Three

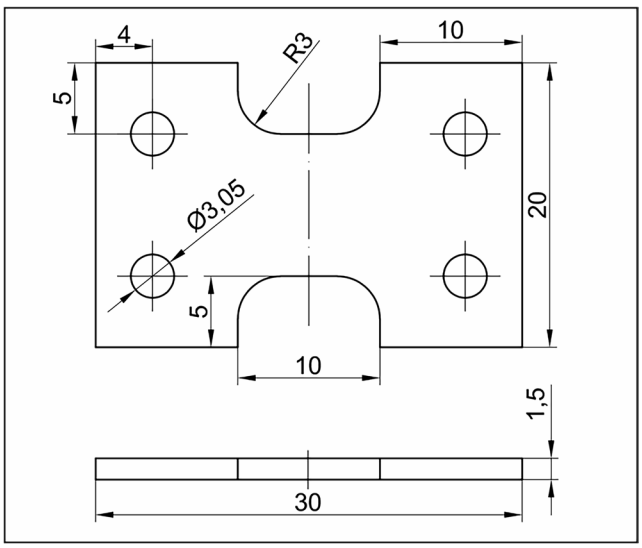

Fig. 1 Geometry of micro tensile test specimen

specimens were tested at each ageing time interval. The data sampling frequency used during the test was 10 Hz. The measurement results were processed using Microstest evaluation software. Additional test parameters: Load cell: 5 kN; Test temperature: room temperature (23 ± 5 °C). The tests were performed with crosshead speed control. The test speed (here: crosshead separation rate) was 1 mm/min.

Since ageing originates from microstructural changes, macroscopic findings, along with microstructural or micromechanical analyses, were also provided. In the context of formability, in addition to evaluating the tendency of mechanical measures, we also examined correlations related to the microstructural relationship based on Hance's [24] method. In the analysis, the Formability Index (FI) and the Local/Global Strain Ratio (L/GSR) demonstrate the combined effect of the raw material's chemical composition and microstructure on formability. Those can be calculated as follows (4–9):

$$\text{Formability Index (FI)} = \sqrt{\epsilon_u \text{TFS}} \tag{4}$$

$$\textit{Local/Global} \text{ Strain Ratio (L/GSR)} = \frac{\text{TFS}}{\epsilon_u} \tag{5}$$

$$\text{True Uniform Strain } (\epsilon_u) = \ln(1 + \frac{UE}{100}) \tag{6}$$

$$\text{True Fracture Strain } (TFS) = \ln\frac{A_0}{A_f} \tag{7}$$

$$\text{Uniform Elongation (UE)} = \frac{L_1 - L_0}{L_0} \tag{8}$$

Where L_0: the gage length, L_1: the elongated length measured at the greatest force, A_0 and A_f are the cross-sectional area before testing and after fracture. A_f can be calculated based on the ASTM E8/E8M suggestion (6):

$$A_f = \frac{1}{6}(t_1 + 4t_2 + t_3)w_f \tag{9}$$

The interpretation of t_1, t_2, t_3 and w_f are shown in Fig. 2.

Global formability is associated with good in-plane forming behaviour, whereas local formability is accompanied by good out-of-plane forming behaviour, for example, bending with high strain gradients in the thickness direction and high local loading at the outer fibre, as well as good stretchability. Therefore, the true uniform strain (εu) is used as a measure for global formability, representing the plane-strain stress state, and the true fracture strain (TFS) is used as a measure for local formability [25].

A higher FI value indicates better formability, while an L/GSR lower value indicates a favorable material property for forming operations with large areas (e.g. deep drawing), while a higher value indicates a favorable material property for forming operations with small areas (e.g. small radius bending).

So far, we have not found any certainty that the FI and L/GSR indicators were used to study ageing. However, we expect them to be a good indicator of changes in the microstructure, which is why we decided to study them.

The image of the fragments of the test specimens was recorded on a 1830 L Amray Scanning Electron Microscope (SEM), then measured by software with an accuracy of 0.01 mm. The focus of the microscope was continuously

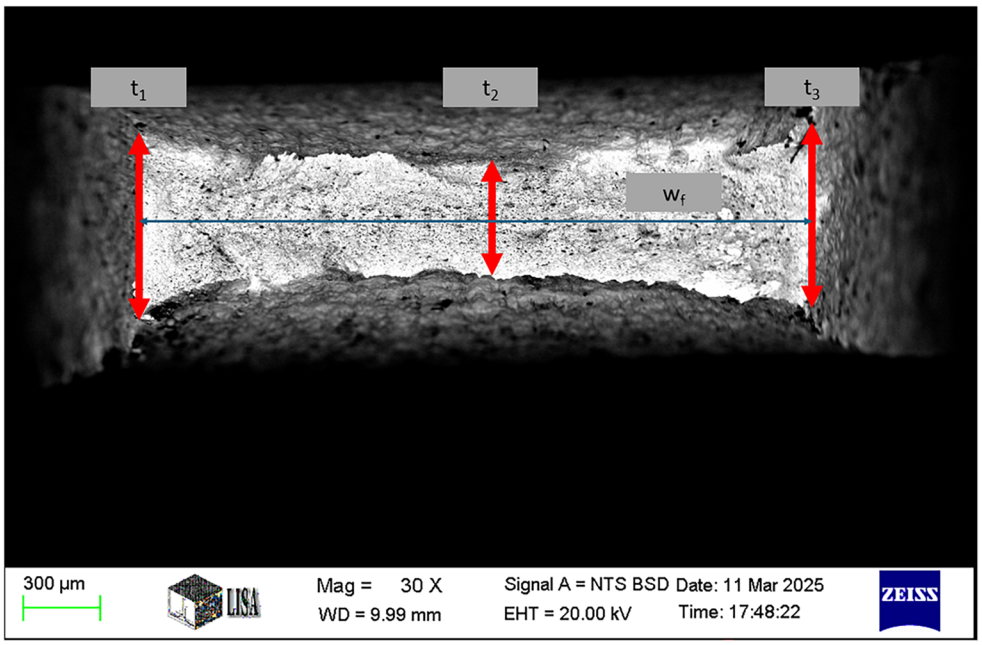

Fig. 2 The interpretation of t_1, t_2, t_3 and w_f on the fractured surface

optimised while the images were being taken. The specimens were fixed on a microscope stage perpendicular to the camera position for the recordings. The near-perfect focus was facilitated by the fact that the tear line of each specimen was at an angle of approximately 55º to the loading axis. The orientation of the specimens was controlled with the naked eye until the sharpest and most complete contour image was obtained. To carry out the measurements as accurately as possible, we drew on the expertise of Wagner and his associates [26].

2.2.4 Deep drawing cup test

The test used the equipment and rules in ISO 11531, with specific boundary conditions. A Roell & Korthaus R21 hydraulic testing device with a die with 33 mm inside diameter and 5 mm rounding radius was used. Before the test, both surfaces of the test piece (circular blank) were coated with lubricant. All measurement parameters and influencing factors specified in the relevant test standard were kept constant during the repeated tests. The tests were always performed by the same person, thus ensuring the repeatability and reproducibility of the tests. At the same time as each series of tensile tests, test pieces were machined from the same sheet as the environment of the tensile test specimens. Four test pieces with gradually increasing diameters between 68 and 74 mm were cut out and drawn into cups at room temperature. Maximum diameter (IG) of the circular blank that can be drawn into a cup was determined as a characteristic parameter of the test.

2.2.5 Nakajima test

The test was carried out using equipment and procedures specified in EN ISO 12004-2. The home-made testing device for the Nakajima tests, consisting of an electro-hydraulic, computer-controlled sheet testing machine and an automated optical deformation measurement system (Fig. 3) is suitable for determining FLC (Forming Limit Curve) diagrams for sheet thicknesses up to 3 mm. We used a 100 mm diameter, hemispherical punch, a matching die and a blankholder. The average punch velocity used in the tests was 1.1 mm/s, while the test temperature was 23 ± 5 °C. We used Teflon foil and graphite lubricant to reduce friction during the test. The forming limit curve is determined by five strain paths, from uniaxial to biaxial tension. The minor true strains (ε2) are plotted on the X axis and the major principal true strains (ε1) on the Y axis. For this purpose, we used the AutoGrid optical measurement system manufactured by VIALUX. The image measurement technique allows the 3D coordinates of the grid points to be determined from images taken from different angles, from which the

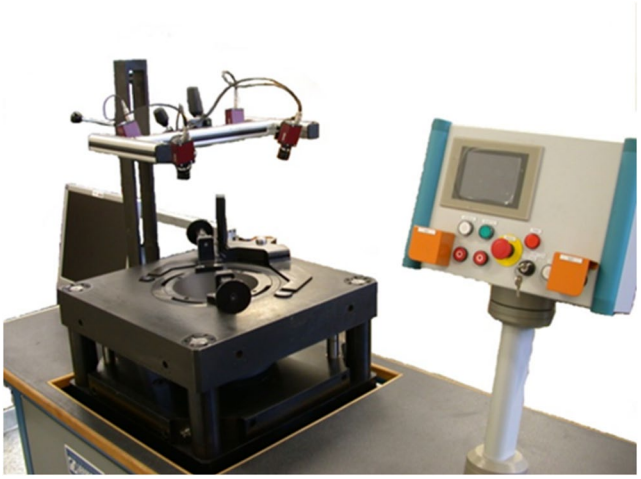

Fig. 3 The home-made universal plate testing device with the Vialux optical measuring system

deformation components can be calculated. The AutoGrid system uses four CCD cameras to determine the strain across the deformed grid. At each ageing time interval, we examined two series of standard test pieces consisting of five pieces each with decreasing parallel shaft widths, those orientations are transversal to the rolling direction (Fig. 4). One series was cut from the edge of the samplesheet and the other from the centre. The shaft widths used were 20 mm, 40 mm, 80 mm, 125 mm, and 200 mm. A printing technique applied a square grid to the prepared test piece series. The grid size used was 2 mm × 2 mm. Before the test, the optical measuring system checked the grid applied to the test piece. The test pieces were prepared by laser cutting. The measurement was performed following the steps: system configuration and calibration; image recording; calculation of the strains. All measurement parameters and influencing factors specified in the relevant test standard were kept constant during the repeated tests. The tests were always performed by the same person, thus ensuring the repeatability and reproducibility of the tests. The rupture of every shaft width specimen starts from the middle of the specimen.

2.2.6 Thermoelectric power measurement

The tests were performed using a TechLab Trivolt PK120 measuring instrument with an accuracy of 2nV/K [27]. The TEP value can be obtained by (10).

$$S = S_p - S_r \tag{10}$$

Where: S_p Seebeck coefficient of the test sample and S_r Seebeck coefficient of the reference wire of the instrument [21]. Two copper blocks were placed on the measuring device used for the tests. One copper block was kept at a

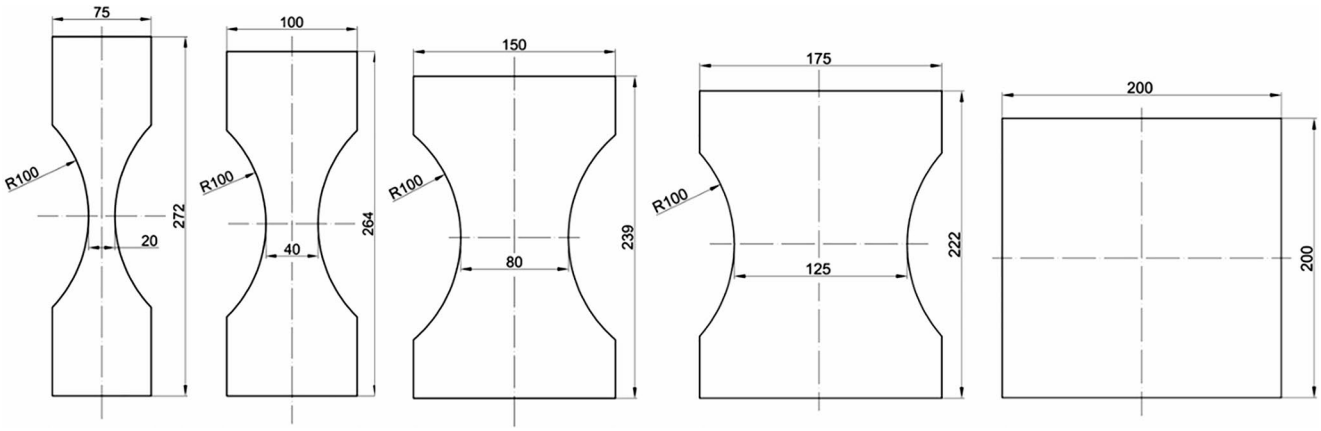

Fig. 4 Geometry of Nakajima test specimens

temperature of 15 °C, while the other was kept at 25 °C by the control electronics. The test sample to be measured was attached to the two copper blocks, causing one end of the test sample to reach a temperature of 15 °C and the other end to reach a temperature of 25 °C. The potential difference between the two ends of the test sample caused by the temperature difference was measured using a low-noise amplifier. Copper reference wires between the amplifier and the copper blocks are used to detect the thermoelectric voltage. Two thermocouples connected in parallel measure the temperature difference at the contact points of the test sample. Since there is no approved standard for this test procedure, the test samples were selected to be identical to those described in the literature [27]. Three test specimens measuring 70 × 5 × 1.5 mm were machined at 0°, 45° and 90° to the rolling direction.

3 Results

3.1 Direct evidence of ageing

We examined the ageing process using two direct methods. In both the 1st and 2nd rounds, we measured the thermoelectric power of our test specimens at 3 days and 6 months of age. The measurements confirmed the ageing process, as the TEP values in the 1st round of tests increased by an average of 82 nV/K, while those in the 2nd round increased by 133 nV/K. The results are consistent with the 160 nV/K increase measured by Mucsi [28] after approximately 9 months, considering that Mucsi and we did not test material from the same supplier, so their interstitial element content was not the same. Regarding the SAI index compared to the reference values of 26–37 MPa reported by Bhagat et al., we measured a value of 90 MPa in our samples, demonstrating our samples' ageing tendency.

3.2 Normal speed tensile test results

In both the 1st and 2nd test rounds, the initial tensile tests were performed on the third day after production, where we confirmed the values specified in the certificate provided by the manufacturer with the coils. We considered this to be the absolute ageing-free initial state. We also examined the initial spread parameter (range) of the mechanical properties of the coil caused by steel manufacturing technology. From the 2nd batch, we cut 160 tensile test specimens from a randomly selected sample sheet parallel to the rolling direction and tested them using normal speed methods. The range of 160 sample results (difference between maximum and minimum values) was 10 MPa for proof strength, 7 MPa for tensile strength, and 4% for elongation.

The changes in mechanical properties, the proof strength, tensile strength and the elongation as a function of storage time are shown in Figs. 5, 6, 7, 8, 9 and 10. All data are averages of 3 sample results. Outliers were examined using the Grubbs test according ISO5725-2 when evaluating the results. Looking at the diagrams, no clear trend emerges as mentioned in the literature. Although in the case of the proof strength (Rp0.2), the value decreases after 3 months in all three directions in the 1st round of samples (Fig. 5), this was not noticeable in the case of tensile strength (Rm) (Fig. 7), and in fact, a slight increase was observed. In the case of elongation after fracture (A80), a slight decrease can be observed in the 1st round of tests compared to the 3-day values (Fig. 9). However, this trend is not apparent in the 2nd round of tests (Fig. 10). After examining the entire data set, from three days to 12 months of, Table 2 shows the intervals obtained in each direction (difference between maximum and minimum values) for the 2nd round specimens. Therefore, in both rounds, the average fluctuations shown in Figs. 5, 6, 7, 8, 9 and 10 are roughly equivalent to the range values measured on the 160 test samples. In other

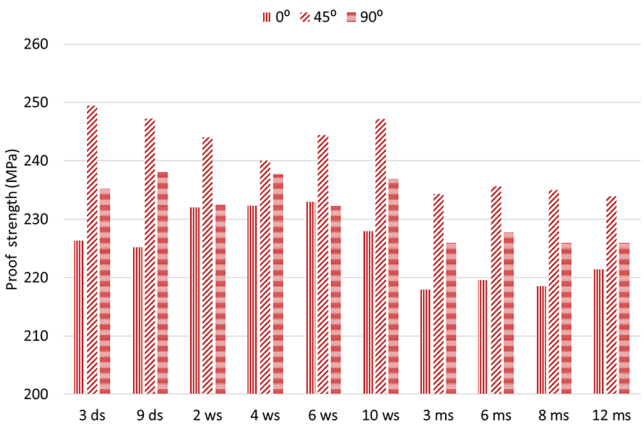

Fig. 5 Proof strength as a function of ageing time (3 days-12 months) in different directions (0°, 45°, 90°), 1st round

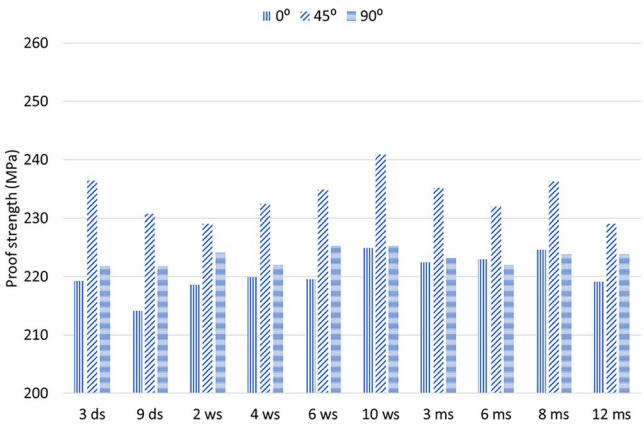

Fig. 6 Proof strength as a function of ageing time (3 days-12 months) in different directions (0°, 45°, 90°), 2nd round

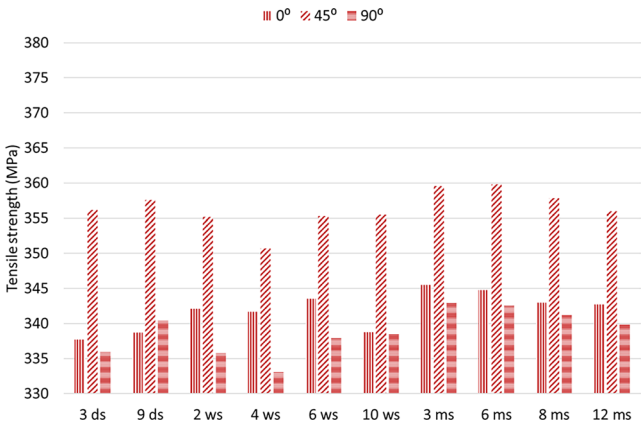

Fig. 7 Tensile strength as a function of ageing time (3 days-12 months) in different directions (0°, 45°, 90°), 1st round

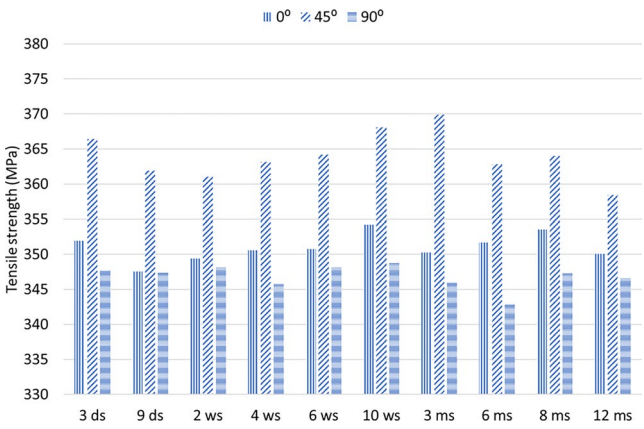

Fig. 8 Tensile strength as a function of ageing time (3 days-12 months) in different directions (0°, 45°, 90°), 2nd round

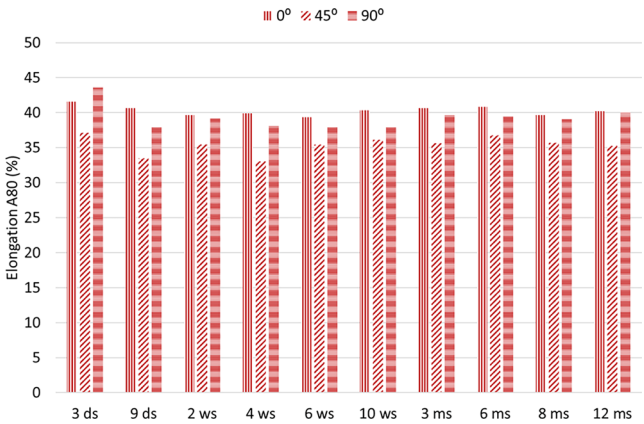

Fig. 9 Elongation as a function of ageing time (3 days-12 months) in different directions (0°, 45°, 90°), 1st round

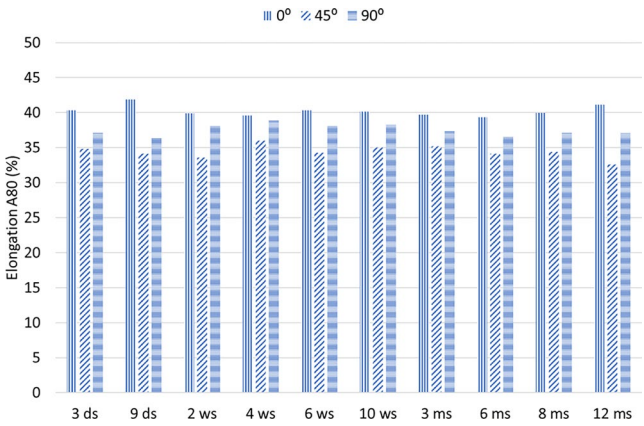

Fig. 10 Elongation as a function of ageing time (3 days-12 months) in different directions (0°, 45°, 90°), 2nd round

Table 2 Intervals (difference between maximum and minimum values) obtained in each direction for the 2nd round in the total storage interval

	direction	
Rp0.2 (MPa)	0 °	6
	45 °	11
	90 °	3
Rm (MPa)	0 °	6
	45 °	8
	90 °	5
A80 (%)	0 °	2
	45 °	2
	90 °	2

words, the normal and reduced speed tensile test shows no signs of ageing.

3.3 Reduced speed tensile test results

In addition to the mechanical values, we also examined the appearance of static and dynamic ageing signs on stress-strain curves recorded at reduced test speeds. Similar to the results of the normal speed tensile tests, no lower or upper yield strength could be determined in any of the approximately 140 measurements, so static ageing could not be determined in this case either, as was the case with the normal test speed tensile tests. The effect of dynamic ageing was examined in the uniform plastic strain range of the stress-strain curve. Although our test covered the entire uniform strain range, for ease of comparison, the results are always shown at the same strain (Fig. 11). These results show that the serrated yielding was only detectable at a test speed of 0.00002 s^{-1}. Even then, it only became visible without magnification at 6 weeks, but this sign remained until 12 months. However, no serration was detectable at faster test speeds! The above-mentioned phenomenon was only observed on the 1st round of test specimens. In contrast, the diagrams of 2nd-round test specimens did not show any serration at any time, even at the lowest test speed.

3.4 Tensile test results extended by digital image correlation technique

During the DIC tests, our attention was limited to studying the phenomena observed at and around the yield point. Static ageing was evaluated at the onset of the yield point, while dynamic ageing was evaluated at 10% strain. The measurement point of 10% was chosen because the hardening exponent is also measured in the uniformplasticstrain range between 10% and 20%. During the tests, the mechanical parameters were not evaluated quantitatively. However, looking at the stress-strain curves, it was clear that neither upper/lower yield point nor a serration developed at any of the ageing time intervals. Nevertheless, on the strain map recorded at the onset of the yield

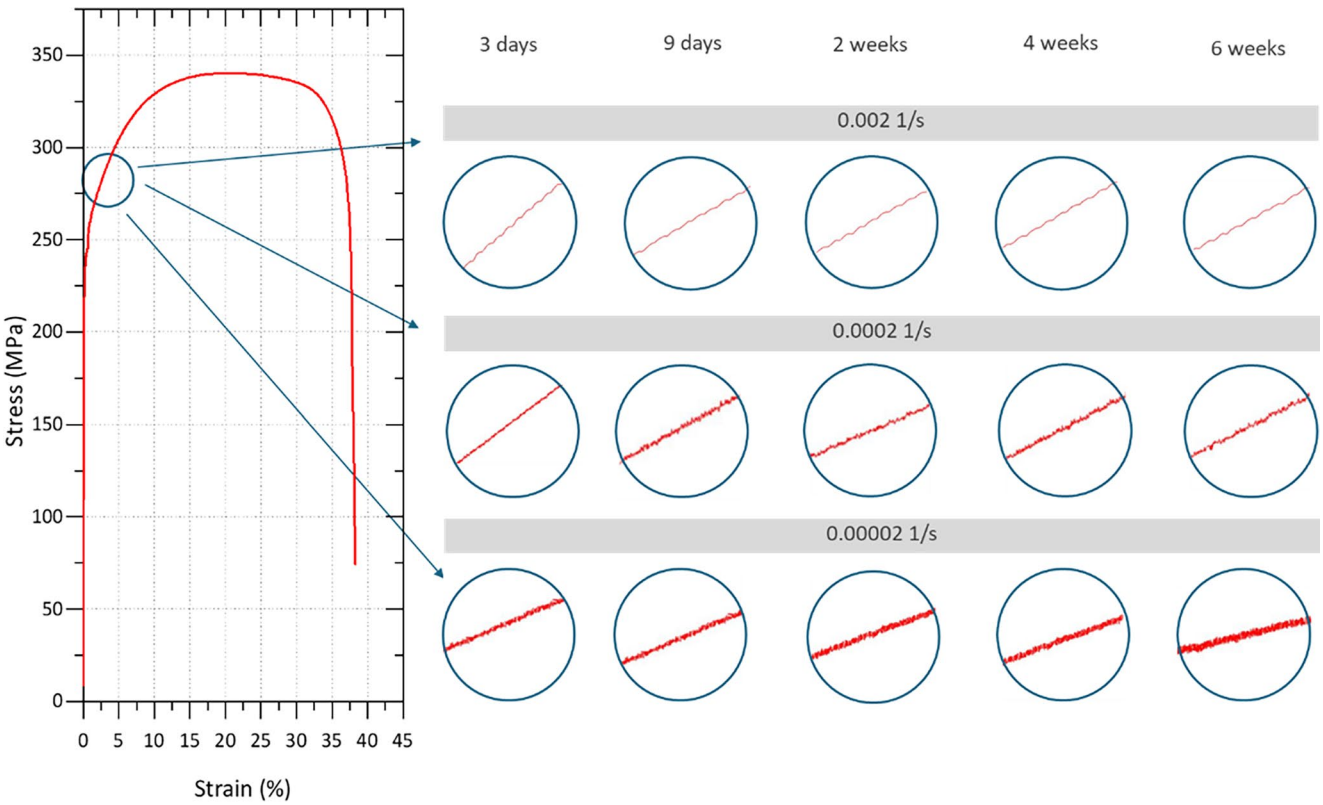

Fig. 11 Signs of dynamic ageing in reduced speed tensile test of 1st round specimens. Test speed 0.002–0.00002 s^{-1}, Ageing time 3 days-6 weeks

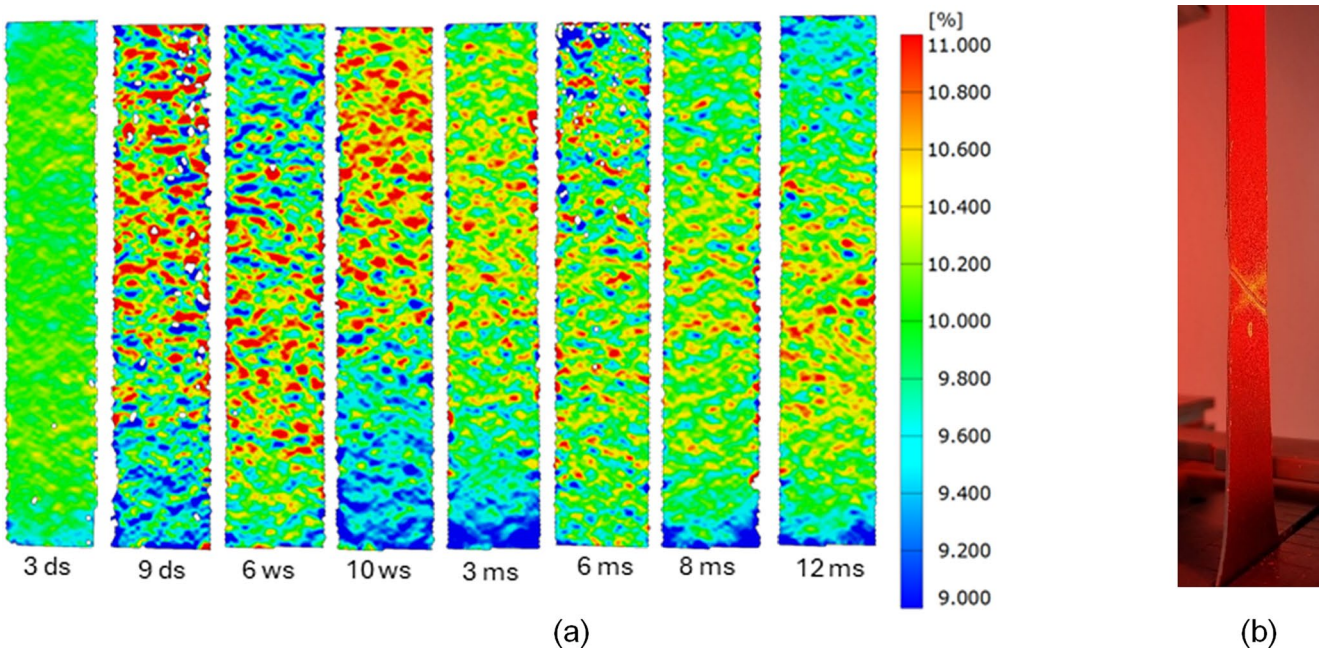

Fig. 12 (**a**) Strain map recorded at the onset of the yield point by DIC, on the surface of the tensile test samples. Ageing time 3 days-12 months, 2nd round (**b**) defect-prone regions on macro photo after fractured sample in the tensile test machine

point, local strain line structures (initial Lüders lines) can be observed, becoming increasingly stronger and denser with time. This phenomenon also appears on the strain maps, which correspond to 10% strain.

Furthermore, it can be seen that the 3-day recording is distinct from the others (Fig. 12(a)). The strain values are much lower on the 3-day test specimen, and the distribution of strains is more uniform. The strains are already higher in the subsequent 9-day recording, and their distribution is more uneven. Interestingly, the higher strain in isolated areas is located in a low-value base matrix. This predicts defect-prone regions during processing (development of visible Lüders lines or cracks (Fig. 12(b)). The striking homogeneity of the 3-day test specimen is also reflected in the low value of the local inhomogeneity factor. The value of Λ becomes exceptionally high from 9 days onwards (Fig. 13).

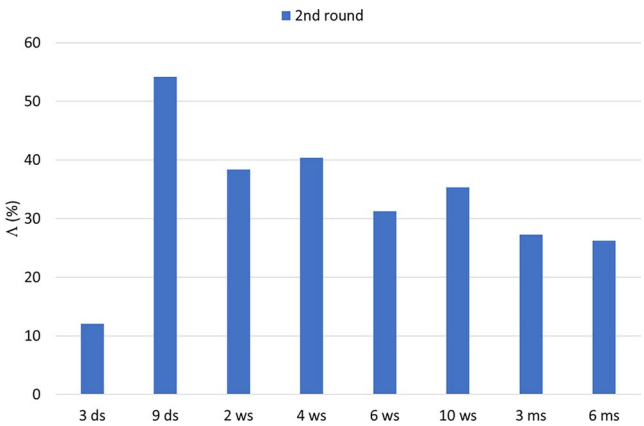

Fig. 13 The local inhomogeneity factor Λ calculated by strain maps of the surface of the tensile test samples. Ageing time 3 days-6 months, 2nd round

3.5 Micro-tensile test results

During this test, we only evaluated the characteristics of the force-displacement curve (Fig. 14). It can be concluded that dynamic ageing occurred in two stages. No deviation was observed in the curve during the 1st two test intervals. However, starting at 1 month of age, a slight but identifiable serration in the uniform strain range appeared, which became markedly stronger at 10 weeks of storage and remained at the same level until the end of the test series at 12 months.

Figure 15 and Fig. 16 show the calculated Formability Index and the Local/Global Strain Ratio by measured from the fracture surface of test specimens. Figures represent the average of three measurements taken at different ageing times. It is obvious that the 3 day sample performs a higher FI value, meaning better formability. It is also associated with the smallest L/GSR value, which indicates a favourable property for forming operations with larger areas (e.g., deep drawing).

Not only the shape of the fractures, but also their morphology, was examined. Scanning Electron Microscopy images (Fig. 17) show that in the case of the 3 days sample, a uniform, ductile fracture surface was formed. At the same time,

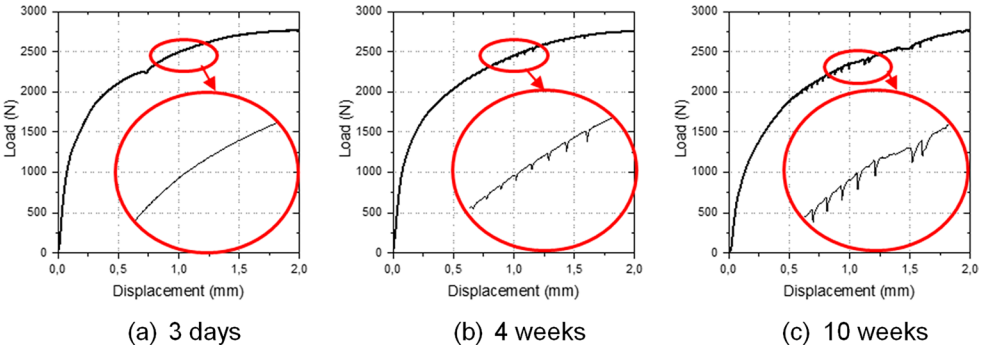

Fig. 14 Signs of dynamic ageing at micro tensile test of 2nd round specimens after (**a**) 3 days (**b**) 4 weeks (**c**) 10 weeks ageing time

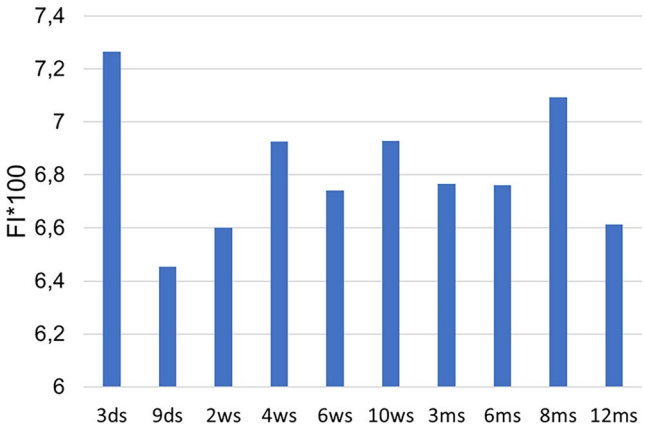

Fig. 15 The Formability Index as a function of ageing time

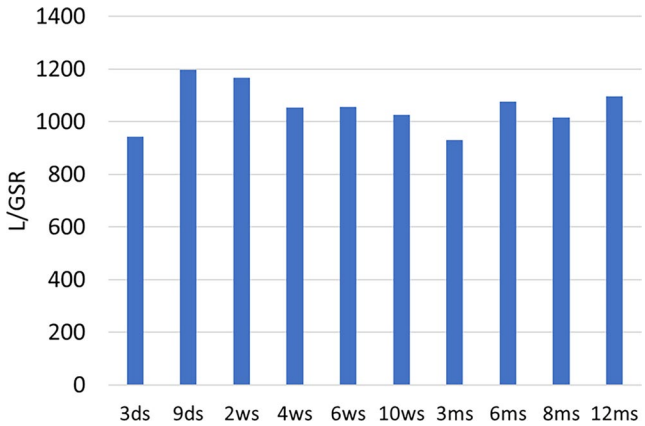

Fig. 16 The L/GSR Index as a function of ageing time

with the onset of ageing, it becomes increasingly characteristic of the fracture surface that the formation of microcavities is banded, with a marked preference for the centerline.

It has been observed in metallurgical tests that nucleation of microvoids and their growth and coalescence are the main steps toward the formation of a mesocrack in ductile materials, which eventually leads to failure. Besides the stress intensity, stress triaxiality has been shown to be the most important factor controlling the initiation of ductile damage. For example, metal forming operations are characterised by low stress triaxiality, which allows for large plastic deformations with minimal damage accumulation (see practical function of the L/GSR value) [29]. The formulation proposed by Gurson was one of the most important coupled damage constitutive models that uses the void volume fraction as an indicator of damage accumulation. Gurson's model has been modified and extended to account for void nucleation and void coalescence, the most prominent of these extensions being the Gurson-Tvergaard-Needleman (GTN) model. The GTN model can accurately predict ductile fracture across a range of medium to high stress triaxiality [30]. From a microstructure perspective, ductile damage occurs in the sequence of void nucleation-void growth-void coalescence (modarete to high triaxialities) or by shear band formation (low triaxialities) [31]. In other words, in ductile fracture, the material separation depends on the local stress and strain states. Due to the pinning effect of interstitial elements on the movement of dislocations, ageing in low-carbon steels alters the local dislocation density, increasing the number of nucleations and raising the stress concentration, which leads to void formation in the microstructure. In Fig. 17 a and b, a certain number of tiny dimples can be observed, which is a typical sign of ductile fracture. In Fig. 17 c-f combinations of brittle and ductile fractures in the same fractured surface can be seen. The brittle fracture particle can be triggered by the existence of strong stress concentration due to ageing.

3.6 Deep drawing cup test results

When evaluating the tests, following today's usual product requirements, only blank diameters that could be pulled into a cup without damage in all three test specimens were accepted as flawless performance. The results of the 1st and 2nd rounds of tests consistently show (Fig. 18) that IG decreases over time, although not to the same extent or at the same rate in the 1st and 2nd rounds. This trend confirms the deterioration of formability.

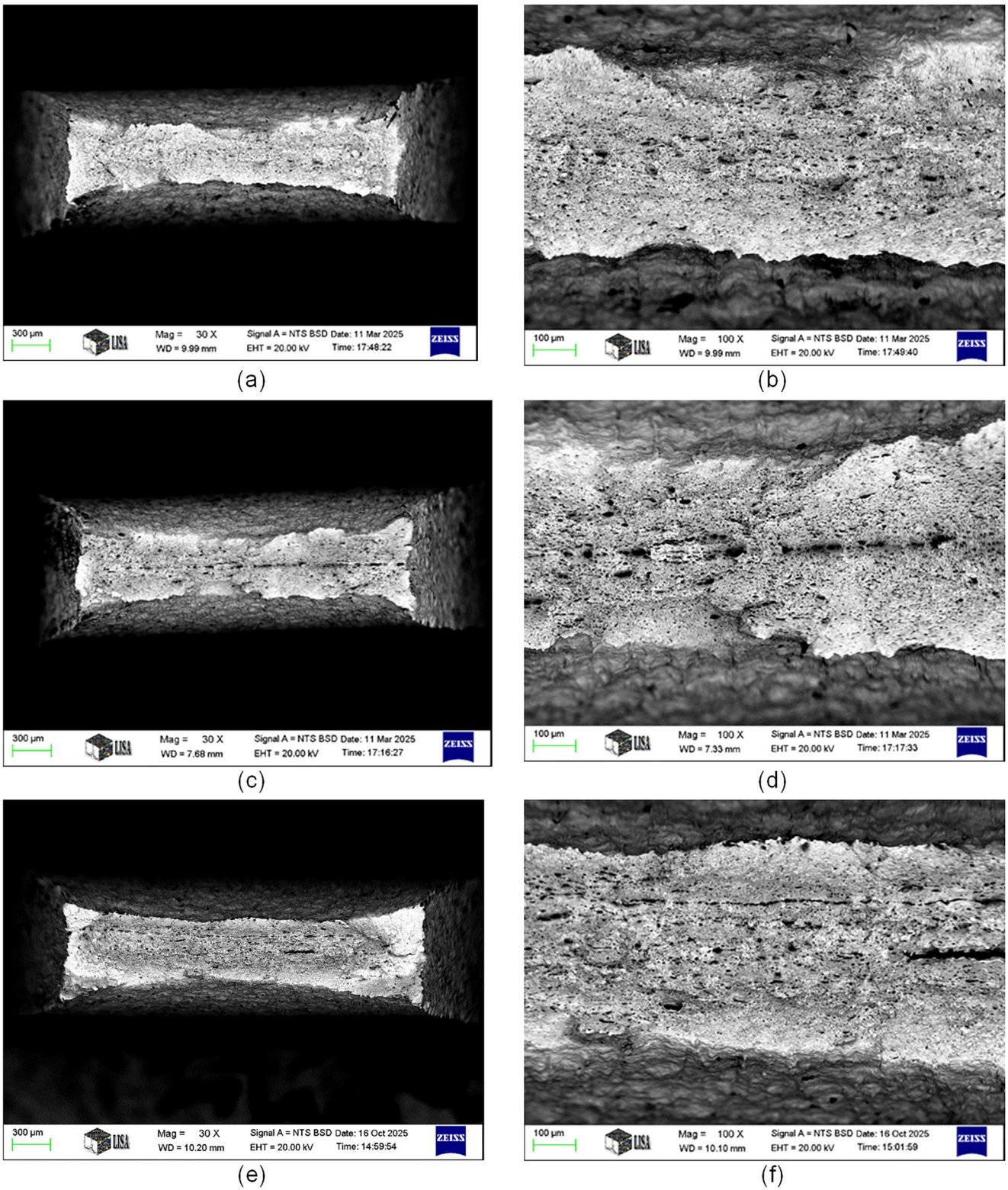

Fig. 17 SEM images of fracture surface of micro tensile test samples of 2nd round specimens after (**a**, **b**) 3 days (**c**, **d**) 4 weeks (**e**, **f**) 3 months ageing time

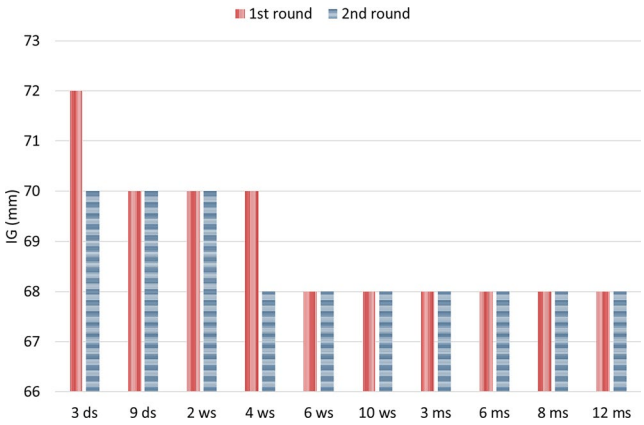

Fig. 18 IG values of deep drawing cup tests after 3 days-12 months ageing

3.7 Nakajima test results

When evaluating the forming limit curves recorded with the Nakajima test (Fig. 19), it was found that there was a significant difference in the slope of the right wing of the curves recorded at each test time between the 3-day and 12-month-old pieces. In contrast, the curves on the left wing did not show any marked trend as a function of storage time. The positions of the left-wing curves are determined by the pieces with smaller shaft widths, which, like the tensile test specimens, are subjected to uniaxial stress. In contrast, the largest pieces with greater shaft widths are subjected to biaxial stress.

We also examined the mode of failure of the Nakajima test specimens by visual inspection. Figure 20 shows an example of how failure changes with advancing age for 200 × 200 mm test specimens. In the case of the 3 days sample, no further surface damage can be seen with the naked eye. After 9 days, flow lines occur almost perpendicular to the center line crack. After 10 weeks, more distant thinning can also be observed. These fracture patterns clearly

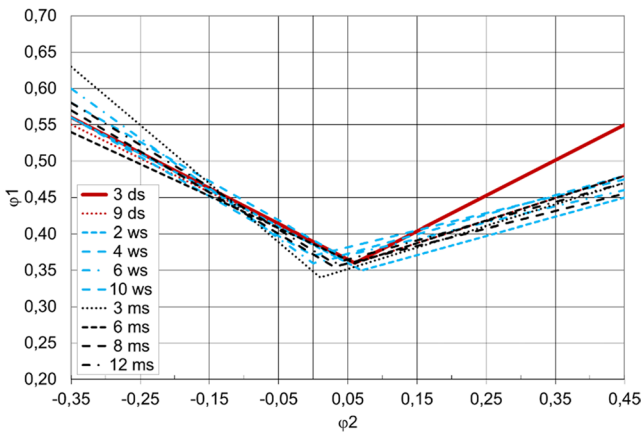

Fig. 19 FLC after 3 days-12 months ageing

illustrate the changes in the failure mode and formability of a practical industrial case. The microstructural changes mentioned in Chap. 3.5 and Fig. 17 were likely also performed on the Nakajima test specimens. During ageing, the global formability of the material decreased; therefore, on the test pieces' surface, damage (so-called distant thinnings) has formed.

4 Discussion

Recurring complaints prompted us to conduct a more in-depth study of strain ageing in an industrial environment. A literature review revealed that previous experiments had evaluated ageing based on standard tensile tests conducted at normal and reduced test speeds. Therefore, our goal was to initiate a complex investigation that would hopefully provide a more accurate picture of the industrial significance of ageing. This expectation was essentially confirmed. Since the start of our experiments, we have conducted 680 tests using eight different test procedures to investigate the ageing behaviour. The large number of tests showed that the ageing of mild steels does not occur at a specific point in time, but rather over a prolonged period, the dynamics of which are also variable. Based on the results of the tests carried out, we can draw the following conclusions:

The progression of ageing could be verified on the 1st and 2nd round of test specimens based on thermoelectric power measurements. In the 2nd round of tests, the fact of ageing was confirmed by the 90 SAI index.

Ageing was more pronounced in the 1st round samples than in the 2nd. This was indicated by a slight decrease in elongation measured on the normal tensile test samples in the 1st round, a slight serrated yielding appeared on the reduced speed stress-strain diagrams, and a steeper decline in the IG values of the deep drawing cup tests. However, the thermoelectric power measurement results showed a slightly greater value in the 2nd round of test samples. The difference may be related to the high sensitivity and locality of the measurement method [32]. In any case, in addition to the above results, the fact that the chemical composition of the 1st round was lower in aluminium and higher in nitrogen than n the 2nd round batch also indicates greater ageing, suggesting that the number of nitrogen atoms capable of free movement may have been higher in the 1st roundbatch.

Based on approximately 360 tensile tests, the increase in proof strength and tensile strength and the decrease in elongation mentioned in the literature as signs of strain ageing were not observed in the tested pieces, nor was the formation of lower and upper yield strength (static ageing).

The serrated yielding known as a dynamic ageing sign in the stress-strain curve was only noticeable in the 1st round

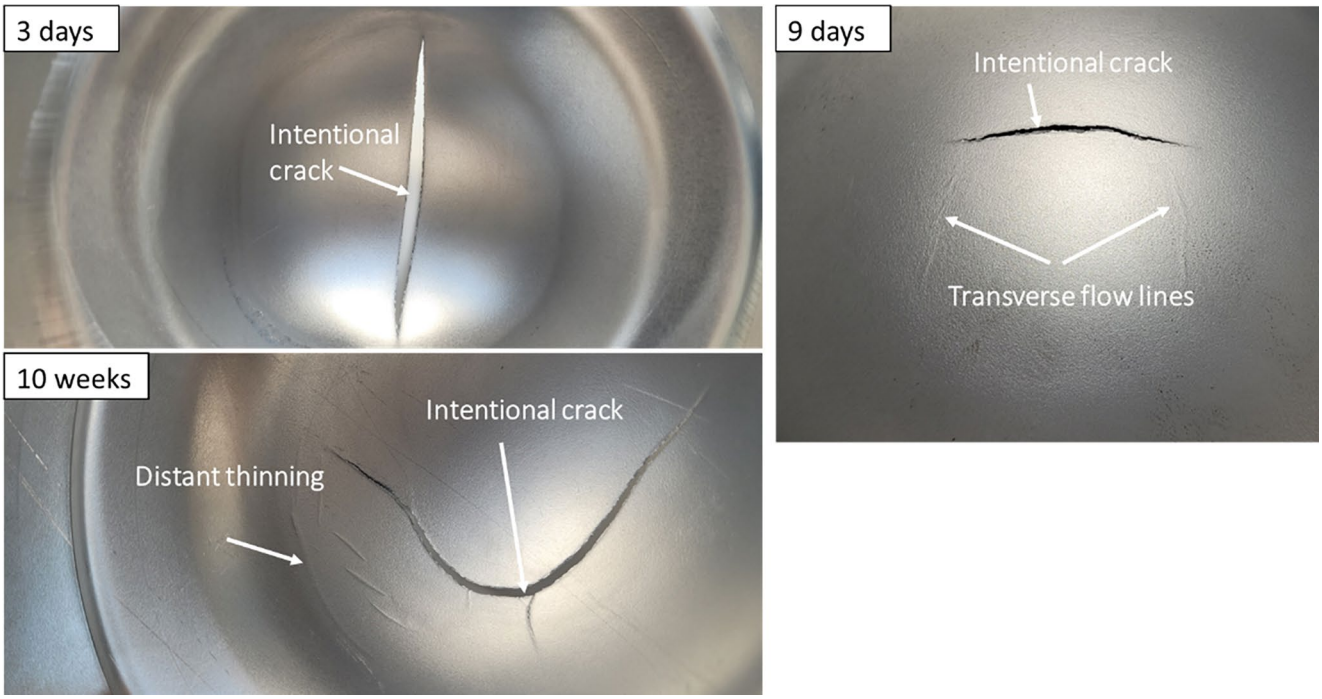

Fig. 20 Failure changes with ageing for 200 × 200 mm Nakajima test specimens

of specimens, which showed greater ageing, six weeks after production, but only at a very low (0.00002 s^{-1}) test speed. This phenomenon only becomes apparent when compared with curves recorded at earlier intervals and is difficult for less experienced employees to recognise.

The tensile test results obtained by the DIC technique were susceptible to ageing. The test clearly showed that the local strain of the 3-day samples was completely homogeneous. At the same time, at 9 days, higher strains began to form in a linear pattern (initial Lüders lines) in the low-value base matrix. This may mean that significant local differences in strains concentrated in a small area may increase the risk of surface damage (visible Lüders lines, local thinning or possibly cracking) during processing. The low value of the local inhomogeneity factor also demonstrates the homogeneity of the 3-day test specimen. The value of Λ then becomes exceptionally high from 9 days onwards.

The micro-tensile test showed that the small test specimen reacted more sensitively to ageing during the test than the standard test specimen in the normal and reduced speed procedures; therefore, the dynamic ageing sign is more easily recognisable from the micro force-displacement curve. The serration appeared in the curve at 1 month and became more pronounced at 10 weeks.

The deep drawing cup test reliably indicated the progression of ageing and thus the deterioration of formability. The results of the 1st round of test pieces showed a two-step change due to greater ageing. The maximum blank diameter (IG) decreased by one test level after 9 days and 6 weeks. In the 2nd round test pieces, the same parameter decreased by one level in a single step at 1 month of age.

The Forming Limit Curves of the Nakajima test for 1st round test pieces also showed signs of ageing. The right-wing of the forming limit curves recorded at each test date shows a significant difference in the slope, whereas the left-wing curves do not show any marked trend as a function of time. The positions of the left-wing curves are determined by the pieces with smaller shaft widths, of which the smallest, similar to the tensile test specimens, are subjected to uniaxial stress. In contrast, the most significant pieces with greater shaft widths are subjected to biaxial stress. This fact confirms our conclusion that the normal and reduced speed tensile test does not respond sensitively enough to changes caused by ageing.

In industrial practice, aging is an unfavorable condition for raw materials, leading to scrap formation in the case of certain combinations of dimensions and designs. To illustrate this, we fed the 3 days and 9 days FLC curves of the 1st round materials into the AutoForm Forming (ver.R12) finite element simulation software as input data to demonstrate the effect of aging in a practical example. The softwere parameters were as follows: aproximation formula of the hardening curve by Combined Swift-Hockett-Sherby (11) and Table 3; Yield Surface: Isotropic Hardening BBC(2005) modell (Table 4).

Table 3 Parameters of hardening curve at the autoform

ϵ_0 [−]	m [−]	C [MPa]	σ_i [MPa]	σ_{sat} [MPa]	a [−]	p [−]	α [−]
0.00648	0.176	559.4	232.1	443.2	6.94	0.786	0.25

Table 4 Parameters of BBC(2005)

r_0 [−]	r_{45} [−]	r_{90} [−]	σ_0/σ_0 [−]	σ_{45}/σ_0 [−]	σ_{90}/σ_0 [−]	σ_b/σ_0 [−]	r_b [−]	M [−]
2.09	1.47	2.44	1.0	1.1609	1.0241	1.1936	0.862	6

$$\sigma = (1-\alpha) \bullet \{C \bullet (\epsilon_{pl} + \epsilon_0)^m\} + \alpha \bullet \left\{\sigma_{sat} - (\sigma_{sat} - \sigma_i)\, e^{-a\epsilon_{pl}^{p}}\right\} \quad (11)$$

Where ε_{pl} is the effective plastic strain. Using the same manufacturing parameters for the design of an everyday mixing bowl, the bowl can be formed without damage from the 3 days material, while the use of the 9 days material results in cracking at the bottom, indicated by the red spot in Fig. 21. During forming, the path taken by the 3 days sample remains below the FLC curve, and the bowl is produced with uniform thinning (braun area). In the case of the 9 days sample, the forming path runs above the right wing of the FLC curve (red dots), resulting in non-linear splits sections (red area on the bowl).

The above results are in line with the restrictions of EN 10,130, which guarantees the proof strength value for only 8 days and recommends that the sheets be processed within 6 weeks. According to this, the DIC tensile test and Nakajima tests, as well as the 1st round of cupping tests, showed deterioration after exactly 9 days, while the reduced speed tensile tests, deep drawing cup tests, and micro-tensile tests showed degradation within a time interval of 4–10 weeks.

5 Conclusion

Our experiments have therefore proven that the currently used definition of ageing needs to be modified and clarified. The fact that the long-used criteria for ageing were not evident in the test samples can be attributed to several reasons. In recent decades, steel manufacturing technology has undergone significant development, enabling the production of cleaner and more homogeneous melts than before. As a result, the nitrogen content of cold-rolled sheets produced using modern technology, including the free nitrogen content, is much lower than it used to be. As a result, ageing is also less pronounced, i.e., the increase in proof strength and the decrease in elongation do not change as much as they did in the past. The changes in the mechanical parameters are so small that they can be covered by the otherwise minor variation caused by the steel manufacturing technology of the sheets (even within a single sheet). The so-called SAI index, which compares the increase in proof strength and tensile strength on the same test specimen before and after artificial ageing, is also not sufficiently expressive in an industrial environment because it does not consider manufacturing inhomogeneity. Therefore, another method and index are needed for the industry to show ageing much more formally and accurately.

Another argument against the industrial application of the SAI measure is that the increase in proof strength resulting from artificial ageing on the same test specimen is less informative for industry, as it is not realistic to take test specimens from every sheet in a shipment during incoming goods inspection and then take new ones at every time interval in order to measure the degree of aging. Individual proof strength measured before the sheets are used cannot be considered authoritative in themselves, as these individual values cannot be compared to a zero-day reference value measured on another test specimen due to the variation in material properties resulting from the steel manufacturing process.

Another frequently mentioned symptom of ageing, the appearance of upper and lower yield strength (static ageing), was not observed in any of the samples tested, possibly because it does not develop with such a small degree of ageing.

The third symptom of ageing frequently mentioned in the literature, the serrated yielding appearing in the tensile diagram (dynamic ageing), could not be confirmed in the normal and only partially in the reduced speed test. In contrast, micro-tensile testing accurately showed the serration that appears over time. The reason for the contradiction with the literature can be found in the size of the test specimens, i.e., while the normal and reduced speed tensile testing specimens were 80 × 20 mm, those for micro-tensile testing were 10 × 5 mm. This means that the micro-tensile test is much more sensitive to the lower degree of ageing observed in steels produced with today's modern technology, and is recommended for determining dynamic ageing rather than the reduced-speed tensile test.

Of the tests presented, the DIC tensile test, micro-tensile test, Nakajima test, and deep drawing cup test reliably demonstrated ageing. Similar to normal tensile tests, one part of the Nakajima test does not respond sensitively enough

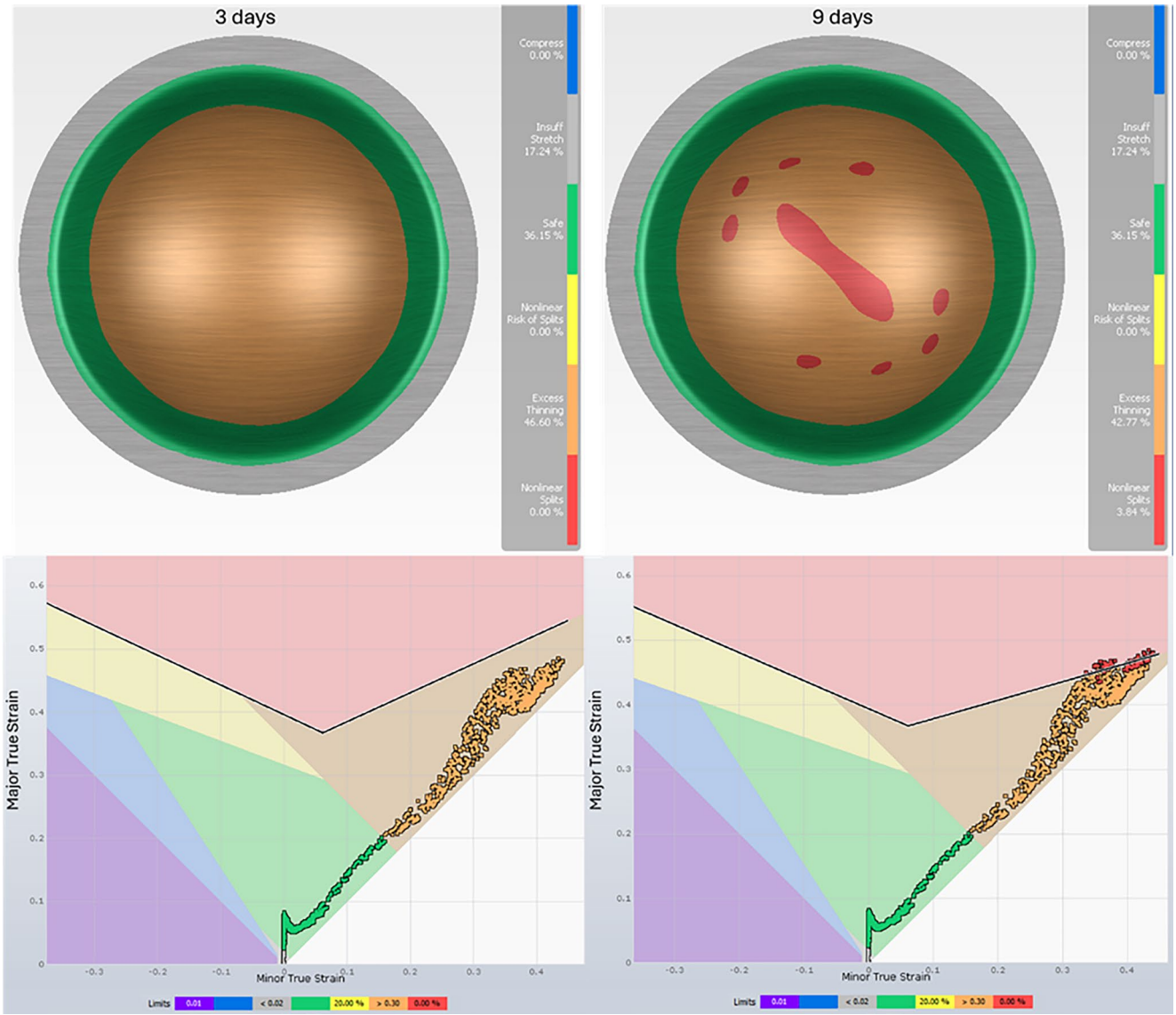

Fig. 21 Finite element simulation of deep drawning process of mixing bowl from 3 days and 9 days old sheet with forming paths and deformation characteristics

to changes. In contrast, deep drawing cup tests provide information on ageing in a highly form-dependent manner. For these reasons, we recommend using the DIC method to determine Λ for industrial characterisation of ageing. The designers must determine their target value individually based on the product's design and the manufacturing technology, using preliminary simulations and experience from trial production and pilot series. Measurement can be easily performed using a camera system adapted to the testing machines commonly used in industry. This investment is justified in cases where damage caused by ageing is of increased importance, e.g. in the case of safety parts or where the cost of production rejects recovers the cost of the camera system in the short term!

6 Summary

Our research investigated the ageing of DC01 grade from two different batches. We showed that the steels are susceptible to ageing using thermoelectric power measurement and the SAI index. The freshly manufactured steels were tested at ages of 3, 9, days, 2, 4, 6, 10 weeks, and 3, 6, 8, and 12 months. We showed that normal and reduced speed tensile tests cannot detect ageing processes. Signs of ageing were detected in the results of tensile tests performed on small test specimens, deep drawing cup tests, and Nakajima tests. Compelling results were obtained from the tensile tests extended with DIC technology, which provided a local strain map and determined the local inhomogeneity factor. Therefore,

we recommend redefining the ageing phenomenon, not as a change in the parameters determined by the tensile test, but as the value of the local inhomogeneity factor. The threshold value should typically be determined based on the service life requirements of the component/consumer goods.

Acknowledgements The authors would like to thank Dr. Zsolt Lukács and Dr. István Mészáros for their contribution to the evaluation of the formability and TEP results, respectively, also for Monika Mende-Tokarova for SEM investigations.

Author contributions B.K. and V.M. wrote the main manuscript, did the conceptualisation. P.K. performed and interpreted the Nakajima and deep drawing tests and related figures such as Fig. 2 and Fig. 3, and provided data for Figs. 14 and 15. T.B. performed the micro tensile tests and prepared the related figures (Fig., Figs. 10 and 13). M.F. and D.N. performed the tensile tests with DIC, evaluated the strain maps, and provided data for Figs. 11 and 12. B.K. performed the rest of the testAll authors reviewed the manuscript.

Funding Open access funding provided by University of Miskolc.

Data availability No datasets were generated or analysed during the current study.

Declarations

Competing interests The authors declare no competing interests.

References

1. De Souza T, Rolfe BF (2010) Characterising material and process variation effects on springback robustness for a semi-cylindrical sheet metal forming process. Int J Mech Sci 52(12):1756–1766 https://doi.org/10.1016/j.ijmecsci.2010.09.009
2. Cottrell AH, Bilby BA (1949) Dislocation theory of yielding and strain ageing of iron. Proc Phys Soc A 62(1):49–62 https://doi.org/10.1088/0370-1298/62/1/308
3. Campbell JD (1953) The dynamic yielding of mild steel. Acta Metall 1(6):706–710 https://doi.org/10.1016/0001-6160(53)90029-7
4. Brindley BJ, Barnby JT (1966) Dynamic strain ageing in mild steel. Acta Metall 14(12):1765–1780 https://doi.org/10.1016/0001-6160(66)90028-9
5. Van Den Beukel A, Kocks UF (1982) The strain dependence of static and dynamic strain-aging. Acta Metall 30(5):1027–1034 https://doi.org/10.1016/0001-6160(82)90211-5
6. Hrivňák A, Sobotová L (1992) The influence of the deformational ageing and the conditions of stress on the properties of the deep-drawing steel sheet. J Mater Process Technol 34(1–4):425–430 https://doi.org/10.1016/0924-0136(92)90137-h
7. De AK, Vandeputte S, de Cooman BC (2001) Kinetics of strain aging in bake hardening ultra low carbon steel - a comparison with low carbon steel. J Mater Eng Perform 10(5):567–575. https://doi.org/10.1361/105994901770344719
8. Silvestre E, Mendiguren J, Galdos L, De Sáenz E (2015) Comparison of the hardening behaviour of different steel families: from mild and stainless steel to advanced high strength steels. Int J Mech Sci 101–102:10–20 https://doi.org/10.1016/j.ijmecsci.2015.07.013
9. Samek L, Dykas J, De Moor E, Grajcar A (2020) Strain-ageing of low-alloyed multiphase high-strength steels. Metals 10(4):439 https://doi.org/10.3390/met10040439
10. Shen Z, Wang B, Liang G, Zhang Y, Han K, Song C (2018) Grain boundary Pop-in, yield point phenomenon and carbon segregation in aged low carbon steel. ISIJ Int 58(2):373–375. https://doi.org/10.2355/isijinternational.isijint-2017-426
11. Bhagat AN, Baek S-J, Lee H-C (2008) A simple method for prediction of shelf life of bake hardening steels. ISIJ Int 48(12):1781–1787. https://doi.org/10.2355/isijinternational.48.1781
12. Sarkar B, Datta R, Chaudhuri SK (2009) Effect of Ti/N ratio on strain aging and plastic anisotropy in extra deep drawing quality steel. Mater Sci Technol 25(11):1408–1410. https://doi.org/10.1179/174328408x363362
13. Wang XG, Wang L, Huang MX (2017) Kinematic and thermal characteristics of Lüders and Portevin-Le Châtelier bands in a medium Mn transformation-induced plasticity steel. Acta Mater 124:17–29 https://doi.org/10.1016/j.actamat.2016.10.069
14. Giarola AM et al (2015) Strain heterogeneities in the rolling direction of steel sheets submitted to the skin pass: A finite element analysis. J Mater Process Technol 216:234–247 https://doi.org/10.1016/j.jmatprotec.2014.09.015
15. Fang S, Zheng X, Zheng G, Zhang B, Guo B, Yang L (2021) A new and direct R-value measurement method of sheet metal based on multi-camera DIC system. Metals 11(9):1401 https://doi.org/10.3390/met11091401
16. Halim H, Wilkinson D, Niewczas M (2007) The Portevin–Le Chatelier (PLC) effect and shear band formation in an AA5754 alloy. Acta Mater 55(12):4151–4160 https://doi.org/10.1016/j.actamat.2007.03.007
17. Qiu H, Inoue T, Ueji R (2020) In-situ observation of Lüders band formation in hot-rolled steel via digital image correlation. Metals 10(4):530 https://doi.org/10.3390/met10040530
18. Guetaz V, Massardier V, Merlin J, Ravaine D, Soler M (2001) Determination of aluminium nitride or free nitrogen in low carbon steel. Steel Res 72(7):245–249 https://doi.org/10.1002/srin.200100112
19. Felde I, Mucsi A (2013) Simulation and measurement of aluminium–nitride precipitation in hot rolled Al killed low carbon steel coil. Int Heat Treat Surf Eng 7(4):172–175 https://doi.org/10.1179/1749514813z.00000000086
20. Massardier V, Lavaire N, Soler M, Merlin J (2004) Comparison of the evaluation of the carbon content in solid solution in extra-mild steels by thermoelectric power and by internal friction. Scr Mater 50(12):1435–1439 https://doi.org/10.1016/j.scriptamat.2004.03.010
21. Mucsi A (2014) Thermoelectric power study of nitride precipitation and recrystallization in continuously-heated low carbon Al-killed steels. Acta Polytech Hung 11(8):87–102 https://doi.org/10.12700/aph.11.08.2014.08.5
22. Fruehan RJ, Steel Foundation AISE (eds) (1998) The making, shaping, and treating of steel, 11th edn. AISE Steel Foundation, Pittsburgh, PA

23. Szalai S, Harangozó D, Czinege I (2020) Characterisation of inhomogeneous plastic deformation of AlMg sheet metals during tensile tests. IOP Conf Ser : Mater Sci Eng 903(1):012023 https://doi.org/10.1088/1757-899X/903/1/012023
24. Hance B (2016) Advanced high strength steel: deciphering local and global formability', in *Proc. International Automotive Body Congress*, Dearborn
25. Heibel S, Dettinger T, Nester W, Clausmeyer T, Tekkaya AE (2018) Damage mechanisms and mechanical properties of high-strength multiphase steels. Materials 11(5):761 https://doi.org/10.3390/ma11050761
26. Wagner L, Larour P (2018) Influence of specimen geometry on measures of local fracture strain obtained from uniaxial tensile tests of AHSS sheets. IOP Conf Ser : Mater Sci Eng 418:012074 https://doi.org/10.1088/1757-899X/418/1/012074
27. Mészáros I, Bögre B, Szabó PJ (2022) Magnetic and thermoelectric detection of sigma phase in 2507 duplex stainless steel. Crystals 12(4):527 https://doi.org/10.3390/cryst12040527
28. Mucsi A (2014) Effect of hot rolled grain size on the precipitation kinetics of nitrides in low carbon Al-killed steel. J Mater Process Technol 214(8):1536–1545 https://doi.org/10.1016/j.jmatprotec.2014.02.024
29. Brünig M, Chyra O, Albrecht D, Driemeier L, Alves M (2008) A ductile damage criterion at various stress triaxialities. Int J Plast 24(10):1731–1755 https://doi.org/10.1016/j.ijplas.2007.12.001
30. Wu H, Zhuang X, Zhao Z (2022) Extended GTN model for predicting ductile fracture under a broad range of stress states. Int J Solids Struct. https://doi.org/10.1016/j.ijsolstr.2022.111452
31. Rickhey F, Hong S (2022) Stress triaxiality in anisotropic metal sheets—definition and experimental acquisition for numerical damage prediction. Materials 15(11):3738 https://doi.org/10.3390/ma15113738
32. Ferrer JP, De Cock T, Capdevila C, García Caballero F, De García C (2007) Comparison of the annealing behaviour between cold and warm rolled ELC steels by thermoelectric power measurements. Acta Mater 55(6):2075–2083 https://doi.org/10.1016/j.actamat.2006.11.010